

Frequency measurement on the $5s5p\ ^3P_2 - 5s4d\ ^3D_3$ transition of ^{88}Sr atoms using the photon-momentum-transfer technique

Koji Hashiguchi,^{1,2,*} Tomoya Akatsuka,^{1,2,†} Noriaki Ohmae,^{1,2} Masao Takamoto,² and Hidetoshi Katori^{1,2}

¹*Department of Applied Physics, Graduate School of Engineering, The University of Tokyo, Bunkyo-ku, Tokyo 113-8656, Japan*

²*Quantum Metrology Laboratory, RIKEN, Wako, Saitama 351-0198, Japan*



(Received 25 September 2019; published 25 October 2019)

We report a frequency measurement on the $5s5p\ ^3P_2 - 5s4d\ ^3D_3$ transition of ^{88}Sr atoms at $2.9\ \mu\text{m}$. The excitation spectra are obtained by measuring the photon momenta transferred to ultracold atoms. The transition frequency is determined to be $102\,550\,196\,205(9)$ kHz using an erbium fiber-based optical frequency comb. We numerically investigate possible frequency corrections by taking an acceleration of atoms and attenuation of the excitation light into account. This measurement technique is particularly useful for transitions where laser-induced fluorescence is difficult to observe but the spatial imaging of atoms is possible.

DOI: [10.1103/PhysRevA.100.042513](https://doi.org/10.1103/PhysRevA.100.042513)

I. INTRODUCTION

The spin-singlet ground state and spin-triplet metastable states in alkaline-earth-metal (like) atoms have been demonstrated as promising transitions for precision measurements, including atom interferometers [1,2], optical lattice clocks [3], and quantum information processing [4–6]. To facilitate such applications, a narrow-line laser cooling [7–11] and an evaporative cooling to Bose-Einstein condensation [12–14] have been developed. By combining cooling transitions starting from the ground and metastable states, continuous laser cooling of atoms down to ultracold temperature will be possible [15–18]. Such an atom source will be of particular importance to improve the stability of atomic clocks and the sensitivity of interferometers by reducing atom preparation time.

Using the $^3P_2 - ^3D_3$ cyclic transitions, laser cooling and trapping of metastable Ca and Mg atoms have been demonstrated at $1.978\ \mu\text{m}$ and at $383\ \text{nm}$ [16–18]. Similarly Sr atoms have metastable $5s5p\ ^3P_0$ and 3P_2 states with lifetimes longer than $100\ \text{s}$ [19,20]. In particular, the $5s5p\ ^3P_2 - 5s4d\ ^3D_3$ transition at $\lambda = 2.923\ \mu\text{m}$ [21,22] offers unique opportunities by exploiting its multiple times longer wavelength λ than that of the visible light: A photon-recoil-limited laser-cooling allows achieving nK regime and its large absorption cross section is conveniently applicable to non-destructive measurements using dispersion of atomic samples [23], as they scale as λ^{-2} and λ^2 , respectively. However, the transition frequency of Sr has so far been measured with an uncertainty of $170\ \text{MHz}$ [22] that is much larger than the natural linewidth of $\gamma/2\pi = 57\ \text{kHz}$ [24].

Transitions between the $5s5p\ ^3P$ and $5s4d\ ^3D$ states for Sr are in the wavelength range of $2.6\text{--}3.1\ \mu\text{m}$, which makes it inconvenient to directly observe laser-induced fluorescence (LIF) due to lack of low-cost imaging devices. In addition, an application of an electron shelving technique [25] is not effective because of their relatively short upper-state lifetimes of a few μs . Optical pumping to conveniently accessible states has been applied to observe such transitions: Frequency measurements on the $5s5p\ ^3P_2 - 5s4d\ ^3D_2$ transition at $3.012\ \mu\text{m}$ have been demonstrated with $80\ \text{MHz}$ uncertainty [26] by monitoring LIF on the $5s^2\ ^1S_0 - 5s5p\ ^1P_1$ transition. The lifetime of the $5s4d\ ^3D_1$ state [27] has been measured by observing fluorescence on the $5s5p\ ^3P_1 \rightarrow 5s^2\ ^1S_0$ transition, after exciting the $5s5p\ ^3P_0 \rightarrow 5s4d\ ^3D_1$ transition at $2.603\ \mu\text{m}$. Such an optical pumping scheme to the ground state is inapplicable to investigate the $5s5p\ ^3P_2 - 5s4d\ ^3D_3$ transition, as it is a cyclic transition.

In this paper, we report the absolute frequency measurement on the $5s5p\ ^3P_2 - 5s4d\ ^3D_3$ transition of ^{88}Sr with an uncertainty of $9\ \text{kHz}$, by applying a photon momentum transfer technique [28,29]. We develop a narrow-linewidth $2.9\ \mu\text{m}$ light source based on the difference frequency generation (DFG) from two frequency-stabilized lasers. After irradiating this probe light onto the ultracold atoms, we measure the photon momenta transferred to the atoms by observing spatial images of atoms using the $5s5p\ ^3P_2 - 5s4d\ ^3D_3$ transition at $496\ \text{nm}$. We thus obtain the photon-momentum-transfer (PMT) spectra with an excellent signal-to-noise ratio. The PMT spectra subject to the blue shift caused by the Doppler shift in the course of the photon momentum transfer. As long as the attenuation of the probe light is negligible [29], this blue shift can be corrected by linearly extrapolating the number of absorbed photons to zero. However, as the atomic density increases, we find this linear extrapolation becomes invalid because of the large absorption cross section in the mid-infrared transition. We calculate the PMT spectra by taking the attenuation of the probe light into account, which reasonably explains the experimentally observed spectra.

*Present address: Gas and Humidity Standards Group, Research Institute for Material and Chemical Measurement, National Metrology Institute of Japan, AIST, Tsukuba, Ibaraki 305-8563, Japan.

†Present address: NTT Basic Research Laboratories, Nippon Telegraph and Telephone Corporation, Atsugi, Kanagawa 243-0198, Japan.

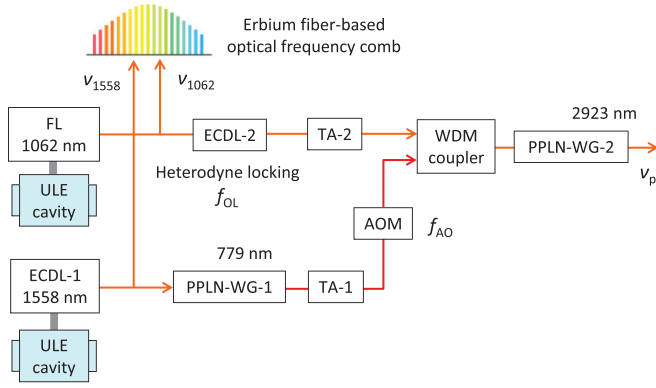


FIG. 1. Generation of narrow-linewidth $2.9\ \mu\text{m}$ light. The frequencies of the two frequency-stabilized lasers at 1062 nm and 1558 nm are measured using an erbium fiber-based optical frequency comb. Two periodically poled lithium niobate waveguides (PPLN-WGs) are used for the second harmonic generation for the 779 nm light and for the difference frequency generation. ECDL, external cavity diode laser; FL, fiber laser; ULE, ultralow expansion; TA, tapered amplifier; AOM, acousto-optic modulator; and WDM, wavelength-division multiplexing.

II. NARROW LINEWIDTH $2.9\ \mu\text{m}$ SOURCE

Figure 1 shows the generation of $2.9\ \mu\text{m}$ probe light using DFG from two lasers at 779 and 1062 nm. An external cavity diode laser (ECDL-1) at 1558 nm and a fiber laser (FL) at 1062 nm are frequency-stabilized to two high-finesse cavities made of ultralow-expansion (ULE) glass. The ECDL-1 is frequency-doubled to 779 nm by a periodically-poled lithium niobate waveguide (PPLN-WG-1) and is amplified by a tapered amplifier (TA-1). An ECDL-2 at 1062 nm is heterodyne-locked to the FL and amplified by a tapered amplifier (TA-2). They are combined by a wavelength-division multiplexing (WDM) coupler and injected into a PPLN-WG-2 for DFG. Input laser power of 100 mW each generates a difference frequency with maximum power of 3.6 mW. The linewidths ~ 200 Hz of the two frequency-stabilized lasers are mainly caused by the Doppler noise in tens-of-meter long optical-fibers used to deliver the lasers. The intensity of the $2.9\ \mu\text{m}$ light is controlled by an acousto-optic modulator (AOM) that attenuates the power of the 779 nm laser.

An erbium fiber-based optical frequency comb [30] is used to measure frequencies. We operate the comb with a repetition frequency $f_{\text{rep}} \approx 68$ MHz and a carrier-envelope offset frequency $f_{\text{ceo}} \approx 46.4$ MHz, where f_{rep} is stabilized by heterodyne-locking a comb line to a frequency-stabilized laser at 1397 nm and f_{ceo} is stabilized to an RF reference signal. The frequencies of the two frequency-stabilized lasers are given by $\nu_{1062} = f_{\text{ceo}} + N_{1062}f_{\text{rep}} + f_{1062}$ and $\nu_{1558} = f_{\text{ceo}} + N_{1558}f_{\text{rep}} + f_{1558}$, where f_{1062} (f_{1558}) is the beat frequency between the frequency-stabilized laser at 1062 nm (1558 nm) and the N_{1062} -th (N_{1558} -th) comb line. By measuring f_{rep} , f_{1062} , and f_{1558} with frequency counters, we obtain the frequency of the probe light $\nu_p = 2\nu_{1558} - \nu_{1062} - f_{\text{OL}} + f_{\text{AO}}$, where f_{OL} is an offset frequency of the ECDL-2 at 1062 nm, and f_{AO} is a frequency shift by the AOM at 779 nm. Reference signals for RF oscillators and frequency counters are provided by a

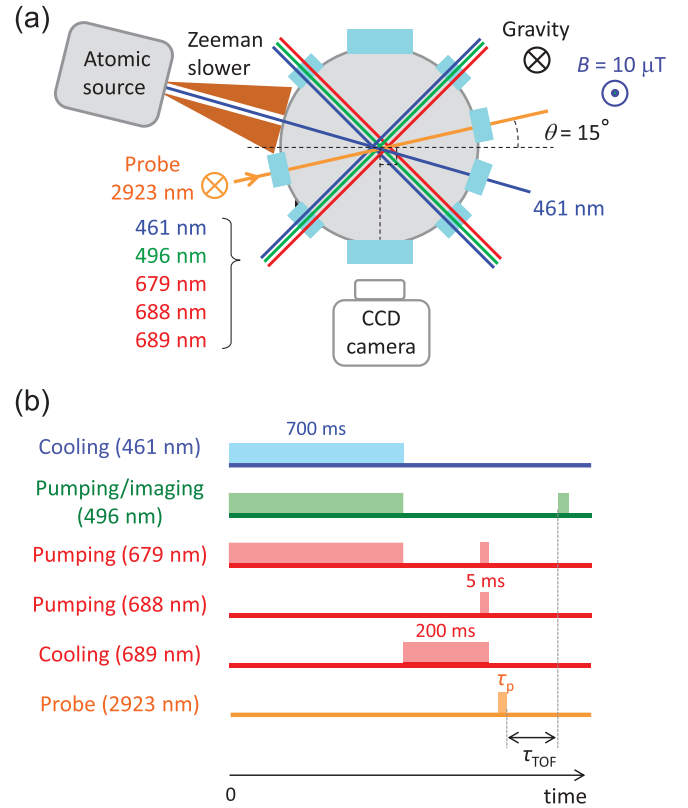


FIG. 2. (a) A schematic of an experimental setup. Atoms are decelerated in a Zeeman slower and trapped at the center of a main chamber. Cooling and pumping beams are combined and introduced into the chamber. An imaging plane for a CCD camera is shown by the dashed line, where the gravity directs downward. A probe light at $\lambda_p = 2.9\ \mu\text{m}$ is incident on atoms horizontally, which intersects with the imaging plane with an angle of $\theta = 15^\circ$. (b) A timing chart for the spectroscopy. Atoms are optically pumped to the 3P_2 state after the second-stage MOT. The probe light pushes the atoms horizontally for τ_p . After a free flight time of τ_{TOF} , spatial images of the atoms are observed by the CCD camera by driving the $^3P_2 - 5s5d^3D_3$ transition at 496 nm.

GPS-disciplined BVA-quartz oscillator with instability $< 10^{-11}$ for an averaging time longer than 1 s.

The probe light is collimated with a $1/e^2$ beam radius of 7 mm and introduced into a vacuum chamber where we prepare ultracold atoms. Because its wavelength is within the absorption band of water, we use vacuum windows made of anhydrous silica glass. The transmission of the anti-reflection coated window is 83%. The maximum intensity applied to the atoms is $I = 3 \times 10^3 I_0$ with $I_0 = 0.3\ \mu\text{W}/\text{cm}^2$ the saturation intensity of the $5s5p^3P_2 - 5s4d^3D_3$ transition.

III. EXPERIMENT

An experimental setup and relevant energy levels for ^{88}Sr atoms are shown in Figs. 2(a) and 3, respectively. Atoms from an oven are decelerated in a Zeeman slower and captured in the first-stage magneto-optical trap (MOT) on the $^1S_0 - ^1P_1$ transition at 461 nm with a natural linewidth of 32 MHz, where atoms are cooled down to a few mK. During the first-stage MOT, we excite the $5s5p^3P_2 - 5s5d^3D_3$ and

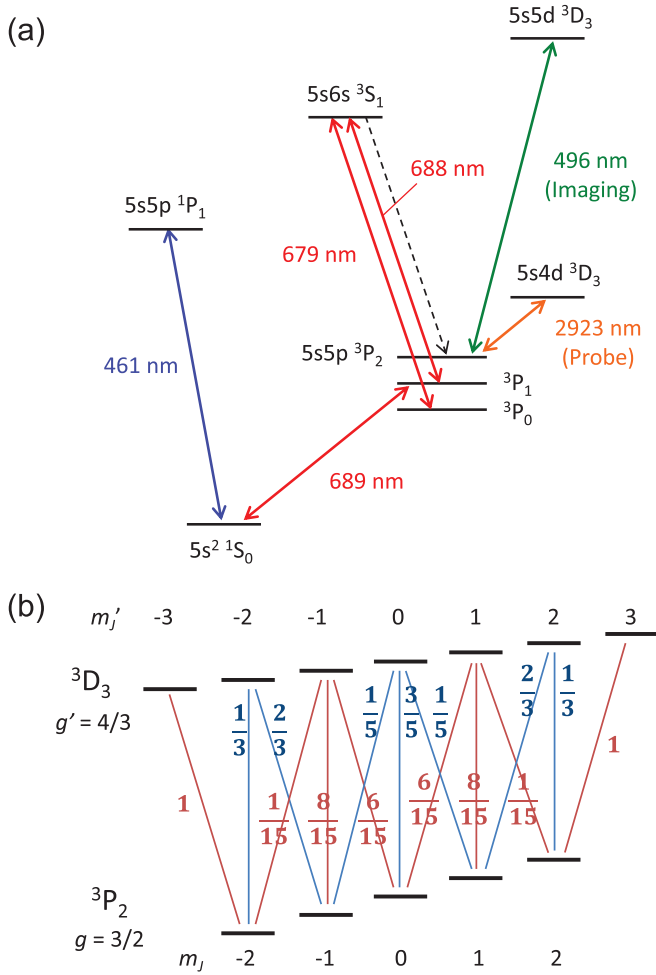


FIG. 3. (a) Relevant energy levels for ^{88}Sr atoms. The two-stage cooling consists of a broad transition at 461 nm and a narrow transition at 689 nm. Transitions at 688 nm and 679 nm are used to optically pump the atoms from the 3P_1 state to the 3P_2 state via the 3S_1 state. Atoms in the 3P_2 metastable state are observed using a transition at 496 nm. (b) The $^3P_2(m_j)$ and $^3D_3(m'_j)$ Zeeman substates with squared Clebsch-Gordan coefficients.

$5s5p^3P_0 - 5s6s^3S_1$ transitions at 496 and 679 nm, respectively, to pump the atoms in the 3P_0 and 3P_2 state back to the ground state. After operating the first-stage MOT for 700 ms, we apply the second-stage MOT [7] for 200 ms to further cool the atoms to a few μK , by employing the $^1S_0 - ^3P_1$ transition at 689 nm with a natural linewidth of 7.5 kHz. At the end of this stage, we transfer the atoms to the 3P_2 metastable state via the 3S_1 state by exciting the $5s5p^3P_1 - 5s6s^3S_1$ and $5s5p^3P_0 - 5s6s^3S_1$ transitions at 688 nm and 679 nm, simultaneously, for 5 ms. We typically obtain $6(3) \times 10^4$ atoms at $4 \mu\text{K}$ in the 3P_2 metastable state. Figure 2(b) depicts a timing chart of the two-stage laser-cooling and spectroscopy.

During spectroscopy, a uniform magnetic field of $B = 10 \mu\text{T}$ is applied in the vertical direction [see Fig. 2(a)] to define the quantization axis and to split the magnetic substates. From a horizontal direction, we apply a π -polarized probe light for $\tau_p = 0.2\text{--}4.0$ ms to excite the $5s5p^3P_2 - 5s4d^3D_3$ transition at $\lambda_p = 2.923 \mu\text{m}$. Consequently, absorbed photons push the atoms horizontally while spontaneously emitted

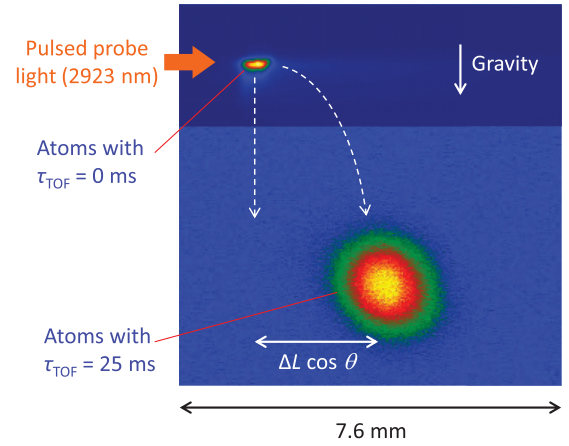


FIG. 4. Images of atoms with a flight time of $\tau_{\text{TOF}} = 0$ and 25 ms. The probe light with pulse width of τ_p pushes the free-falling atoms in the horizontal direction.

photons isotropically kick the atoms. We measure photon momenta transferred to the atoms by a time-of-flight (TOF) technique: After a free-flight time of τ_{TOF} , spatial images of the atoms in the 3P_2 state are observed by a CCD camera by driving the $^3P_2 - 5s5d^3D_3$ transition at 496 nm with a natural linewidth of 9.7 MHz.

Typical CCD images of atoms are shown in Fig. 4. The spatial displacement ΔL of the atoms after $\tau_{\text{TOF}} = 25$ ms in the horizontal direction is determined by a Gaussian fitting where we correct the viewing angle $\theta = 15^\circ$ of the CCD camera [see Fig. 2(a)]. The number of absorbed photons per an atom is given by $n_p = m\lambda_p \Delta L / (h\tau_{\text{TOF}})$ with m the mass of ^{88}Sr , and h the Planck constant.

IV. RESULTS AND DISCUSSIONS

Figure 5(a) shows the number of absorbed photons n_p after applying near-resonant probe light for $\tau_p = 1$ ms. Each point is obtained by averaging five images as illustrated in Fig. 4. We vary the probe intensity as $\epsilon I/I_0 = 50, 28, 16, 9.5,$ and 5.5 indicated by different colors from red to blue shown from top to bottom. Here, ϵ accounts for 50% uncertainty in estimating the probe intensity, which is introduced in measuring its power, beam radius, and position of the beam in respect to the atoms. Note that the relative intensities are precisely measured with uncertainty less than 5%. We experimentally determine ϵ as described later.

For higher probe intensities I , the spectral width is mainly determined by the power-broadening $\gamma(1 + I/I_0)^{1/2}/2\pi$ of the transition. The line shape of the PMT spectrum is primarily affected by the Doppler shift given by the photon recoils, which pushes the peak of the spectra toward the higher frequency. The Doppler broadening (16 kHz at $4 \mu\text{K}$) and a single-photon recoil shift $\nu_R = h/(2m\lambda_p^2) = 0.26$ kHz are smaller than the natural linewidth $\gamma/2\pi$ of the transition.

We numerically simulate the PMT spectra using the rate equations. In particular, we take into account the attenuation of the probe light by an atomic sample with the column number density Q_a , which accounts for atomic-density-dependent frequency shift as we discuss later. Figure 6 shows a model used for the calculation. The probe light propagates along the

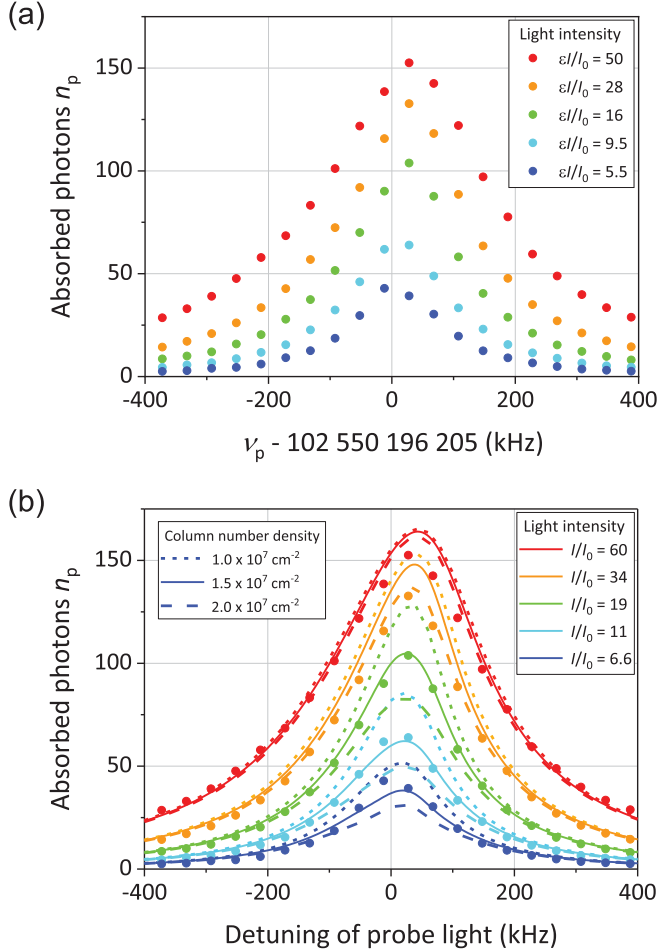


FIG. 5. (a) Observed PMT spectra. The number of absorbed photons n_p is measured for a pulse duration of $\tau_p = 1$ ms. Frequency of the probe light ν_p is determined by the frequency comb. Colors of the symbols correspond to the probe intensities $\epsilon I/I_0 = 50$ (indicated by red), 28, 16, 9.5, and 5.5 (blue) shown from top to bottom, where ϵ accounts for the intensity measurement uncertainty of 50%. (b) Calculated PMT spectra with the probe light intensities $I/I_0 = 60$ (indicated by red), 34, 19, 11, and 6.6 (blue) shown from top to bottom, which reasonably fit experimental data (filled symbols) by taking $\epsilon = 0.83$. Spectral profiles are calculated for column densities $Q_a = 1.0 \times 10^7 \text{ cm}^{-2}$ (dotted lines), $1.5 \times 10^7 \text{ cm}^{-2}$ (solid lines) and $2.0 \times 10^7 \text{ cm}^{-2}$ (dashed lines).

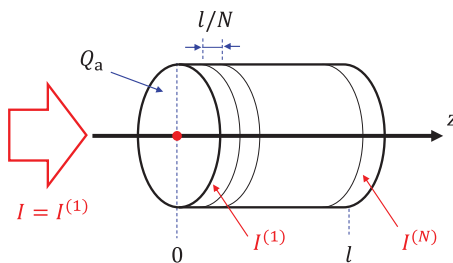


FIG. 6. A model used for the calculation. Atoms are to be assumed uniformly distributed from $z = 0$ to l with a column number density Q_a . The atomic cloud is divided into N segments with a thickness l/N , where the probe light intensity is assumed to be constant within each segment.

z direction and is incident onto atoms uniformly distributed from $z = 0$ to l . The atomic sample is divided into N segments with a thickness l/N . We assume that the probe intensity is constant within each segment, $I(z) = I^{(i)}$ for $(i-1)l/N \leq z < il/N$ with integer $i = 1, 2, \dots, N$, and $I^{(1)} = I$, where the superscript (i) denotes the i th segment.

The atomic populations $n_{m_j}^{P(i)}(t)$ and $n_{m_j}^{D(i)}(t)$ in the ${}^3P_2(m_j)$ and ${}^3D_3(m_j)$ states at time t in the i th segment are given by

$$\frac{dn_{m_j}^{P(i)}(t)}{dt} = -R_{m_j}^{(i)}(t)[n_{m_j}^{P(i)}(t) - n_{m_j}^{D(i)}(t)] + \sum_{m_j'} \gamma C_{m_j, m_j'}^2 n_{m_j'}^{D(i)}(t), \quad (1)$$

$$\frac{dn_{m_j}^{D(i)}(t)}{dt} = R_{m_j}^{(i)}(t)[n_{m_j}^{P(i)}(t) - n_{m_j}^{D(i)}(t)] - \gamma n_{m_j}^{D(i)}(t), \quad (2)$$

where $C_{m_j, m_j'}$ is the Clebsch-Gordan coefficient between the Zeeman substates as shown in Fig. 3(b). By exciting the π transitions, the spontaneous emissions push the atomic populations toward the inner Zeeman states, which reduces the Zeeman broadening of the spectrum.

The optical pumping rate $R_{m_j}^{(i)}(t)$ for the π -transitions is given by [31]

$$R_{m_j}^{(i)}(t) = \frac{I^{(i)}(t)}{2I_0} \frac{\gamma^3 C_{m_j, m_j}^2}{\gamma^2 + 4[\Delta_p - \Delta_B(m_j) - \Delta_D^{(i)}(t)]^2}, \quad (3)$$

where $\Delta_p/2\pi = \nu_p - \nu_0$ is the detuning of the probe light from the resonant frequency ν_0 , $\Delta_B(m_j)/2\pi = (g' - g)\mu_B m_j B/h \approx -23 m_j \text{ kHz}$ gives the Zeeman shift with Landé g -factors $g \approx 3/2$ ($g' \approx 4/3$) for the 3P_2 (3D_3) states, and μ_B denotes the Bohr magneton. The Doppler $\Delta_D^{(i)}(t)/2\pi = 2\nu_R n_p^{(i)}(t)$ is proportional to the number of absorbed photons $n_p^{(i)}(t)$ that obeys the rate equation given by

$$\frac{dn_p^{(i)}(t)}{dt} = \sum_{m_j} R_{m_j}^{(i)}(t)[n_{m_j}^{P(i)}(t) - n_{m_j}^{D(i)}(t)]. \quad (4)$$

By taking the attenuation in the $(i-1)$ th segment into account, the light intensity $I^{(i)}(t)$ for the i th segment is given by

$$I^{(i)}(t) = I^{(i-1)}(t) \exp\left[-\frac{Q_a}{N} \sigma_p^{(i-1)}(t)\right], \quad (5)$$

where $\sigma_p^{(i)}(t)$ is the absorption cross section for the i th segment at t given by

$$\sigma_p^{(i)}(t) = \sum_{m_j} \frac{3\lambda_p^2}{2\pi} \frac{\gamma^2 C_{m_j, m_j}^2 [n_{m_j}^{P(i)}(t) - n_{m_j}^{D(i)}(t)]}{\gamma^2 + 4[\Delta_p - \Delta_B(m_j) - \Delta_D^{(i)}(t)]^2}. \quad (6)$$

We finally obtain the number of absorbed photons per atom $n_p(t)$ as

$$n_p(t) = \frac{1}{N} \sum_{i=1}^N n_p^{(i)}(t). \quad (7)$$

Assuming all Zeeman substates m_j in the 3P_2 state are equally populated $n_{m_j}^{P(i)}(0) = 0.2$ at $t = 0$, and $n_{m_j}^{D(i)}(0) = 0$

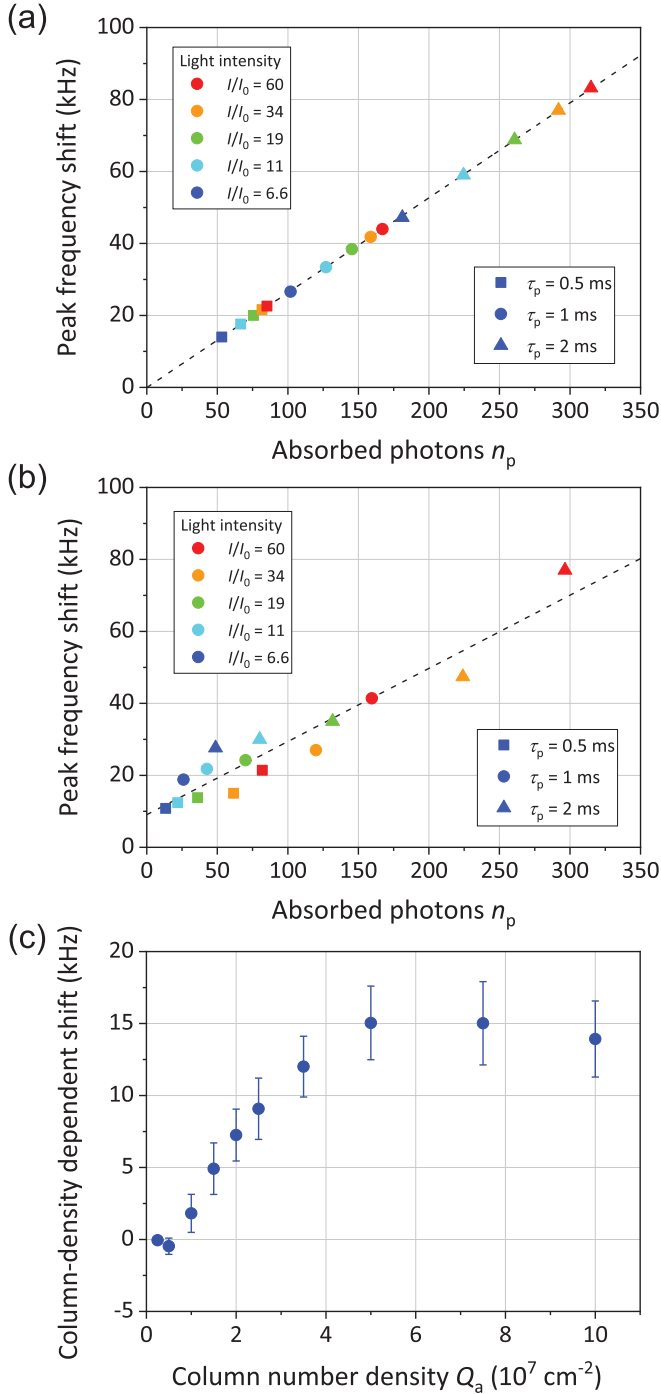


FIG. 7. Peak frequency shift of the PMT spectra as a function of absorbed photons n_p calculated for column number densities (a) $Q_a = 2.5 \times 10^6 \text{ cm}^{-2}$ and (b) $Q_a = 2.5 \times 10^7 \text{ cm}^{-2}$. Colors of the symbols correspond to the probe intensities as shown in legends. Shapes of the symbols indicate the pulse width $\tau_p = 0.5$ ms (square), 1 ms (circle), and 2 ms (triangle). The dashed lines linearly extrapolate $n_p \rightarrow 0$ to remove frequency shift. (c) Column-density dependent frequency offset is summarized as a function of Q_a .

and $n_p^{(i)}(0) = 0$, we calculate the number of absorbed photons $n_p(\tau_p)$ for $N = 10$. Figure 5(b) shows the calculated spectra for probe light intensities $I/I_0 = 60$ (indicated by red), 34, 19, 11, and 6.6 (blue) shown from top to bottom, and col-

umn number densities $Q_a = 1.0 \times 10^7 \text{ cm}^{-2}$ (dotted lines), $1.5 \times 10^7 \text{ cm}^{-2}$ (solid lines) and $2.0 \times 10^7 \text{ cm}^{-2}$ (dashed lines). As shown by the plot, the atomic density effects are less pronounced for the probe detuning $|\Delta_p| > 200 \text{ kHz}$. Using this frequency range, we determine $\epsilon = 0.83$ so as to best fit the experimental line shapes (shown by filled symbols) to the calculation. Next, we compare calculated and measured spectra for the probe detuning $|\Delta_p| < 200 \text{ kHz}$, where the atomic density critically affects the spectral line shapes, to determine $Q_a = 1.5(5) \times 10^7 \text{ cm}^{-2}$. This column density is consistent with $Q_a^{\text{CCD}} = N_a/A = 4(2) \times 10^7 \text{ cm}^{-2}$ that is estimated by CCD images with the number of atoms $N_a = 6(3) \times 10^4$ and the area of ellipse $A = \pi(0.23 \text{ mm}) \times (0.21 \text{ mm})$. Because of the relatively large measurement uncertainty of Q_a^{CCD} , we take Q_a , as obtained in Fig. 5(b), in the following discussion.

We numerically investigate the influence of the light attenuation in the determination of the resonant frequency. Figures 7(a) and 7(b) show the peak frequency shifts of the PMT spectra as a function of absorbed photons n_p for column number densities $Q_a = 2.5 \times 10^6 \text{ cm}^{-2}$ and $Q_a = 2.5 \times 10^7 \text{ cm}^{-2}$, respectively. Colors of the symbols correspond to the probe intensities that are same as used in Fig. 5(a). Shapes of the symbols indicate the pulse width of $\tau_p = 0.5, 1,$ and 2 ms. The dashed lines linearly extrapolate $n_p \rightarrow 0$ to remove frequency shift. While the peak frequency shifts are proportional to n_p for a lower density $Q_a = 2.5 \times 10^6 \text{ cm}^{-2}$, a frequency offset of about 10 kHz appears for $Q_a = 2.5 \times 10^7 \text{ cm}^{-2}$. Figure 7(c) summarizes the frequency offset as a function of the column density. The column-density dependent shifts become constant for $Q_a > 5 \times 10^7 \text{ cm}^{-2}$. In this range, the optical depth becomes more than 10 for the probe light intensities $I < 19I_0$. Consequently, the probe light is entirely absorbed by the atoms in the earlier sections (see Fig. 6), the atoms in the latter sections are not affected by the probe light, which leads to the saturation of the column-density dependent shift.

Figure 8 shows the peak frequencies of the PMT spectra as a function of absorbed photons n_p , measured for an

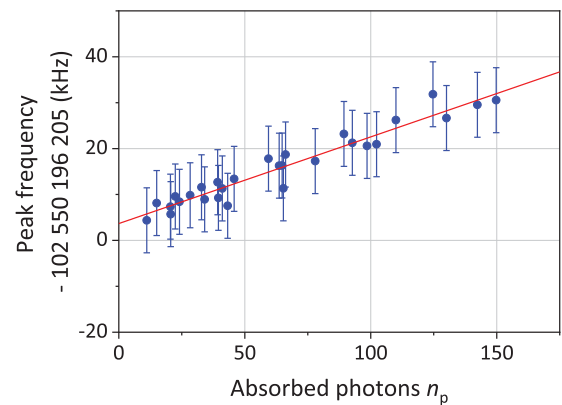


FIG. 8. Peak frequency of the spectrum as a function of absorbed photons n_p , measured for the atomic cloud with $Q_a = 1.5(5) \times 10^7 \text{ cm}^{-2}$. We apply the probe light for $\tau_p = 0.2\text{--}4.0$ ms. The probe intensities are the same as those in Fig. 5(a). The solid line linearly extrapolate $n_p \rightarrow 0$.

TABLE I. Uncertainty budget for the frequency measurement.

Contributor	Standard uncertainty (kHz)
2.9 μm light frequency	7
Estimation of center frequency	2
Zeeman shift	<1
Column-density dependent shift	3
Total	9

atomic sample with $Q_a = 1.5(5) \times 10^7 \text{ cm}^{-2}$. The frequency shift is nearly proportional to n_p . However, the column-density dependent shift exists as discussed above. According to Fig. 7(c), we estimate the column-density dependent shift to be 5(3) kHz.

Table I shows the uncertainty budget. The main contributor is the absolute frequency measurement with an uncertainty of 7 kHz, which is limited by the determination of f_{rep} with an uncertainty of 1 MHz and by the frequency drift ($\sim\text{kHz/h}$) of the probe light. Asymmetric population distribution among the Zeeman substates m_J introduced by residual circular-polarization components may cause a frequency shift. We estimate the residual σ^\pm circular components are less than 3% as the Zeeman components at around $\pm 140 \text{ kHz}$ corresponding to $m_J = \pm 2 \rightarrow m'_J = \pm 3$ transitions are not visible in Fig. 5(a). In addition, relatively large Zeeman shift of $\Delta_B^\pm(m_J)/2\pi \approx -23(m_J \mp 8) \text{ kHz}$ for the σ^\pm circular components, compared to the spectral linewidth, effectively suppresses the optical pumping by the residual circular light near $\Delta_p = 0$. Numerical simulations show that the frequency shift due to the residual circular components is as small as -0.058 kHz , assuming $I/I_0 = 50$ that contains 3% of σ^+ component. For low probe intensities, as the number of optical pumping cycles $\propto n_p$ is limited, an initial distribution among the magnetic substates may cause the frequency shift. Including these sources of uncertainties, we estimate the overall Zeeman shift to be less than 1 kHz.

Figure 9 summarizes the $5s5p^3P_2 - 5s4d^3D_3$ transition frequency obtained by five separate measurements with $Q_a = 1.5(5) \times 10^7 \text{ cm}^{-2}$ (data 1–4) and $1.0(3) \times 10^8 \text{ cm}^{-2}$ (data 5). The red open circles are obtained by linear extrapolation of the experimental data as shown in Fig. 8. The extrapolated frequency obtained in data 5, which is higher by about 10 kHz than the others, coincides with the measurements 1–4 after correcting the column-density dependent shift as given in Fig. 7(c). This indicates the validity of our model that treats the density dependent frequency shifts. In terms of peak atomic density ρ , the data 1–4 and 5 are measured with $\rho = 1.0(5) \times 10^9 \text{ cm}^{-3}$ and $7(4) \times 10^9 \text{ cm}^{-3}$, respectively. Collisional frequency shifts beyond the measurement uncertainty of 9 kHz is not observed in these atomic densities. The average frequency obtained by measurements 1–5 determines the transition frequency to be $\nu_0 = 102\,550\,196\,205(9) \text{ kHz}$, which reduces the uncertainty by more than 4 orders of magnitude in comparison with the reference value of $102\,550\,490(170) \text{ MHz}$ [22].

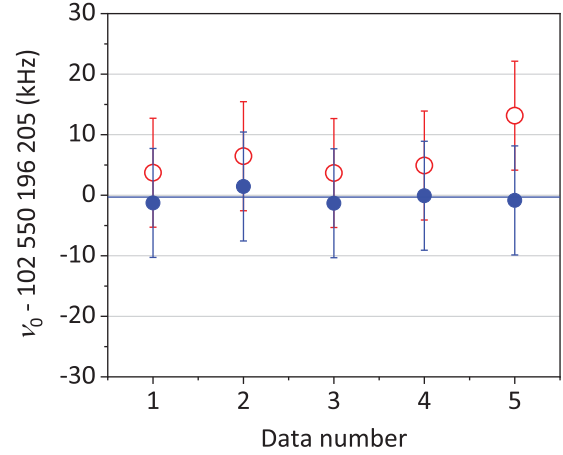


FIG. 9. The $5s5p^3P_2 - 5s4d^3D_3$ transition frequency of ^{88}Sr . Data 1–4 are measured with $Q_a = 1.5(5) \times 10^7 \text{ cm}^{-2}$ and Data 5 is measured with $Q_a = 1.0(3) \times 10^8 \text{ cm}^{-2}$. The filled and open circles show the results with and without column-density corrections. Error bars indicate the combined standard uncertainty. The average of data 1–5 determines the frequency to be $\nu_0 = 102\,550\,196\,205(9) \text{ kHz}$ as indicated by a horizontal line.

V. SUMMARY AND OUTLOOK

We have measured the $5s5p^3P_2 - 5s4d^3D_3$ transition frequency of ^{88}Sr atoms by applying the photon momentum transfer technique. The technique allows detecting the excitations with a good signal to noise ratio as the measurement of the spatial distribution of atoms is insensitive to intensity and frequency fluctuations of the imaging laser. With a help of theoretical model that takes the attenuation of the probe light into account, we have identified the column-density dependent frequency shift that appears in the PMT spectra.

The technique can be useful to measure transitions where direct detection of laser-induced fluorescence is difficult, but the spatial imaging of atoms is possible. The midinfrared transition explored in this work will open up new possibilities. Using Sr atoms in the 3P_2 metastable state, laser cooling toward photon-recoil limited temperature of tens of nK and continuous cooling using electronic state transfer [15] will be possible. In addition, an order of magnitude larger optical depth in the mid-infrared transitions than that for visible transitions will be conveniently applied to the non-destructive measurement of atoms [23]. Both of them will be exploited to further improve the stability of optical lattice clocks.

Note added in proof. Recently, we noticed that magneto-optical trapping of ^{87}Sr atoms on the $5s5p^3P_2 - 5s4d^3D_3$ transition was reported in Ref. [32].

ACKNOWLEDGMENTS

This work is supported by JST ERATO Grant No. JPM-JER1002 10102832 (Japan), by JSPS Grant-in-Aid for Specially Promoted Research Grant No. JP16H06284, and in part by a Grant-in-Aid for JSPS Fellows. The authors acknowledge H. Inaba for preparing the optical frequency comb.

- [1] F. Riehle, T. Kisters, A. Witte, J. Helmcke, and C. J. Borde, *Phys. Rev. Lett.* **67**, 177 (1991).
- [2] G. Ferrari, N. Poli, F. Sorrentino, and G. M. Tino, *Phys. Rev. Lett.* **97**, 060402 (2006).
- [3] H. Katori, M. Takamoto, V. G. Pal'chikov, and V. D. Ovsinnikov, *Phys. Rev. Lett.* **91**, 173005 (2003).
- [4] G. K. Brennen, I. H. Deutsch, and P. S. Jessen, *Phys. Rev. A* **61**, 062309 (2000).
- [5] A. J. Daley, M. M. Boyd, J. Ye, and P. Zoller, *Phys. Rev. Lett.* **101**, 170504 (2008).
- [6] A. V. Gorshkov, A. M. Rey, A. J. Daley, M. M. Boyd, J. Ye, P. Zoller, and M. D. Lukin, *Phys. Rev. Lett.* **102**, 110503 (2009).
- [7] H. Katori, T. Ido, Y. Isoya, and M. Kuwata-Gonokami, *Phys. Rev. Lett.* **82**, 1116 (1999).
- [8] T. Binnewies, G. Wilpers, U. Sterr, F. Riehle, J. Helmcke, T. E. Mehlstaubler, E. M. Rasel, and W. Ertmer, *Phys. Rev. Lett.* **87**, 123002 (2001).
- [9] E. A. Curtis, C. W. Oates, and L. Hollberg, *Phys. Rev. A* **64**, 031403(R) (2001).
- [10] T. Mukaiyama, H. Katori, T. Ido, Y. Li, and M. Kuwata-Gonokami, *Phys. Rev. Lett.* **90**, 113002 (2003).
- [11] E. A. Curtis, C. W. Oates, and L. Hollberg, *J. Opt. Soc. Am. B* **20**, 977 (2003).
- [12] Y. Takasu, K. Maki, K. Komori, T. Takano, K. Honda, M. Kumakura, T. Yabuzaki, and Y. Takahashi, *Phys. Rev. Lett.* **91**, 040404 (2003).
- [13] S. Kraft, F. Vogt, O. Appel, F. Riehle, and U. Sterr, *Phys. Rev. Lett.* **103**, 130401 (2009).
- [14] S. Stellmer, B. Pasquiou, R. Grimm, and F. Schreck, *Phys. Rev. Lett.* **110**, 263003 (2013).
- [15] H. Katori, T. Ido, Y. Isoya, and M. Kuwata-Gonokami, *AIP Conf. Proc.* **551**, 382 (2001).
- [16] J. Grünert and A. Hemmerich, *Phys. Rev. A* **65**, 041401(R) (2002).
- [17] C. Y. Yang, P. Halder, O. Appel, D. Hansen, and A. Hemmerich, *Phys. Rev. A* **76**, 033418 (2007).
- [18] M. Riedmann, H. Kelkar, T. Wübbena, A. Pape, A. Kulosa, K. Zipfel, D. Fim, S. Rühmann, J. Friebe, W. Ertmer *et al.*, *Phys. Rev. A* **86**, 043416 (2012).
- [19] S. G. Porsev and A. Derevianko, *Phys. Rev. A* **69**, 042506 (2004).
- [20] M. Yasuda and H. Katori, *Phys. Rev. Lett.* **92**, 153004 (2004).
- [21] C. E. Moore, *Atomic Energy Levels*, Natl. Bur. Stand. (U.S.) Circ. 467 (U.S. GPO, Washington, DC, 1952), Vol. II.
- [22] J. E. Sansonetti and G. Nave, *J. Phys. Chem. Ref. Data* **39**, 033103 (2010).
- [23] J. Lodewyck, P. G. Westergaard, and P. Lemonde, *Phys. Rev. A* **79**, 061401(R) (2009).
- [24] M. S. Safronova, S. G. Porsev, U. I. Safronova, M. G. Kozlov, and C. W. Clark, *Phys. Rev. A* **87**, 012509 (2013).
- [25] W. Nagourney, J. Sandberg, and H. Dehmelt, *Phys. Rev. Lett.* **56**, 2797 (1986).
- [26] P. G. Mickelson, Y. N. M. de Escobar, P. Anzel, B. J. DeSalvo, S. B. Nagel, A. J. Traverso, M. Yan, and T. C. Killian, *J. Phys. B* **42**, 235001 (2009).
- [27] T. L. Nicholson, S. L. Campbell, R. B. Hutson, G. E. Marti, B. J. Bloom, R. L. McNally, W. Zhang, M. D. Barrett, M. S. Safronova, G. F. Strouse *et al.*, *Nat. Commun.* **6**, 6896 (2015).
- [28] D. S. Weiss, B. C. Young, and S. Chu, *Phys. Rev. Lett.* **70**, 2706 (1993).
- [29] K. Hueck, N. Luick, L. Sobirey, J. Siegl, T. Lompe, H. Moritz, L. W. Clark, and C. Chin, *Opt. Express* **25**, 8670 (2017).
- [30] Y. Nakajima, H. Inaba, K. Hosaka, K. Minoshima, A. Onae, M. Yasuda, T. Kohno, S. Kawato, T. Kobayashi, T. Katsuyama *et al.*, *Opt. Express* **18**, 1667 (2010).
- [31] J. I. Kim, D. Haubrich, B. Klöter, and D. Meschede, *Phys. Rev. A* **80**, 063801 (2009).
- [32] W. Bowden, R. Hobson, I. R. Hill, A. Vianello, M. Schioppo, A. Silva, H. S. Margolis, P. E. G. Baird, and P. Gill, *Sci. Rep.* **9**, 11704 (2019).